IMPLEMENTING MULTI-SCALE AGRICULTURAL INDICATORS EXPLOITING SENTINELS

PRODUCT USER MANUAL

LEAF AREA INDEX (LAI)
FRACTION OF PHOTOSYNTHETICALLY ACTIVE RADIATION (FAPAR)
FRACTION OF VEGETATION COVER (FCover)
From Landsat-8

IMAGINES_RP6.3_PUM_LAI30M

ISSUE I1.00

EC Proposal Reference N° FP7-311766

Due date of deliverable: June 2015

Actual submission date: June 2015

Start date of project: 01.11.2012   Duration : 40 months

Name of lead partner for this deliverable: INRA

Book Captain: Fred baret (INRA)

Contributing Authors: Wenjuan Li (INRA)

Marie Weiss (INRA)

Project co-funded by the European Commission within the Seventh Framework Program (2007-2013)		
Dissemination Level		
PU	Public	**X**
PP	Restricted to other programme participants (including the Commission Services)	
RE	Restricted to a group specified by the consortium (including the Commission Services)	
CO	Confidential, only for members of the consortium (including the Commission Services)	

DOCUMENT RELEASE SHEET

Book Captain:	F. Baret	Date: 27.07.2015	Sign.
Approval:	R. Lacaze	Date: 13.10.2015	Sign.
Endorsement:	I. Marin-Moreno	Date:	Sign.
Distribution:	Public		

CHANGE RECORD

Issue/Revision	Date	Page(s)	Description of Change	Release
	27.07.2015	All	Initial issue	I1.00

TABLE OF CONTENTS

LIST OF FIGURES

LIST OF TABLES

LIST OF ACRONYMS

AD	Additive wavelength dependent noise
AI	Additive wavelength independent noise
ALA	Average leaf angle
ATBD	Algorithm Theoretical Based Document
DN	Digital Number
DHP	Digital Hemispherical Photographics
ECV	Essential Climate Variable
ENVI	Environment for Visualizing Images
ESU	Elementary Sampling Unit
EU	European Union
FAPAR	Fraction of Absorbed Photosynthetically Active Radiation
FCover	Fraction of vegetation cover
GAI	Green Area Index
GCOS	Global Climate Observation System
GEO	Group on Earth Observations
GEOV1	VGT bioGEOphysical product Version 1 (geoland2 project)
GEOV2	VGT bioGEPphysical product Version 2 (geoland2 project)
GEOV3	PROBA-V bioGEOphysical product Version 3 (ImagineS project)
GEOGLAM	Global Agricultural Geo-Monitoring Initiative
GTOS	Global Terrestrial Observation System
HOT	Hot spot parameter
INRA	Institut National de Recherche Agronomique
LAI	Leaf Area Index
LDAS	Land Data Assimilation System
MACCS	Multi-mission Atmospheric and Cloud Correction Software
MD	Multiplicative wavelength dependent noise
MI	Multiplicative wavelength independent noise
MODIS	Moderate-Resolution Imaging Spectroradiometer
NIR	Near Infrared spectral domain
NN	Neural Network
PAR	Photosynthetically Active Radiation
PROSAIL	PROSPECT + SAIL mode
PROSPECT	Proprietes spectrales (a model of leaf optical properties)
PROBA-V	VEGETATION sensor on Project for OnBoard Autonomy platform
PUM	Product User Manual
QA	Quality Assessment
QFLAG	Quality Flags
RMSE	Relative Mean Square Error
SAIL	Scattering by Arbitrarily Inclined Leaves
SWIR	Short Wave Infrared
SZA	Sun Zenith Angle

SAA	Sun Azimuth Angle
TOC	Top of Canopy
USGS	United States Geological Survey
VALERI	Validation of Land European Remote sensing Instruments
VGT	VEGETATION sensor onboard SPOT satellites
VZA	Viewing Zenith Angle
VAA	Viewing Azimuth Angle

1. BACKGROUND OF THE DOCUMENT

1.1. EXECUTIVE SUMMARY

The Copernicus program is the EU response to the increasing demand for reliable environmental data. The objective of the Copernicus Land Service is to continuously monitor and forecast the status of land territories and to supply reliable geo-information to decision makers, businesses and citizens to define environmental policies and take right actions. ImagineS intends to continue the innovation and development activities to support the operations of the Copernicus Global Land service, preparing the use of the new Earth Observation data, including Sentinels missions data, in an operational context. Moreover, ImagineS aims to favor the emergence of downstream activities dedicated to the monitoring of crop and fodder production, that are key for the implementation of the EU Common Agricultural Policy, of the food security policy, and could contribute to the Global Agricultural Geo-Monitoring Initiative (GEOGLAM) coordinated by the intergovernmental Group on Earth Observations (GEO).

The main objectives of IMAGINES are to (i) improve the retrieval of basic biophysical variables, mainly LAI, FAPAR and the surface albedo, identified as Terrestrial Essential Climate Variables, by merging the information coming from different sensors (PROBA-V and Landsat-8) in view to prepare the use of Sentinel missions data; (ii) develop qualified software able to process multi-sensor data at the global scale on a fully automatic basis; (iii) complement and contribute to the existing or future agricultural services by providing new data streams relying upon an original method to assess the above-ground biomass, based on the assimilation of satellite products in a Land Data Assimilation System (LDAS) in order to monitor the crop/fodder biomass production together with the carbon and water fluxes; (iv) demonstrate the added value of this contribution for a community of users acting at global, European, national, and regional scales.

Thus, ImagineS has set-up an algorithm to retrieve the basic biophysical variables from Landsat-8 surface reflectance data at 30 m resolution. The considered products are the following variables: LAI and FAPAR that are Essential Climate Variables (ECVs) as recognized by international organizations such as GCOS and GTOS. In addition, the FCover variable is generated since it corresponds to specific needs for some users. The associated uncertainty and the quality flag are also generated. These products will be combined with GEOV3 products in the further decametric - hectometric fusion algorithm to generate every 10 days decametric products.

The Product User Manual (PUM) describes the LAI, FAPAR and FCover products, derived from Landsat-8 surface reflectance data at 30m resolution. These products are located over eight IMAGINES demonstration sites on original Landsat-8 measurement dates. They are provided in multi-band ENVI standard format, containing the variable values (LAI,

FAPAR and FCover), quality assessment (QA) indicators for per product and quality flags (QFLAG).

1.2. SCOPE AND OBJECTIVES

The PUM is a self-contained document which gathers all necessary information to use the product on an efficient and reliable way. It gives an overview of the products properties, in terms of algorithm, technical characteristics and main validation results.

1.3. CONTENT OF THE DOCUMENT

The document is structured as follows:

- Chapter 2 summarizes the algorithm.
- Chapter 3 describes the technical characteristics of the products.
- Chapter 4 presents the quality assessment of the products.

1.4. RELATED DOCUMENTS

1.4.1. Inputs

Overview of deliverables acting as inputs to this document.

Document ID	Descriptor
ImagineS_RP1.1	User Requirements Document
ImagineS_RP1.2	Service Specifications Document
ImagineS_RP2.1_ATBD-LAI300m	ATBD of LAI, FAPAR, FCover at 300m from PROBA-V (GEOV3)
ImagineS_RP5.1	Detailed Processing Model
ImagineS_RP2.1_ATBD-LAI30m	ATBD of LAI, FAPAR, FCover at 30m from Landsat-8

2. ALGORITHM

The algorithm, defined by INRA (Institut National de Recherche Agronomique), generates the leaf area index (LAI), the Fraction of absorbed PAR (FAPAR) and the fraction of vegetation cover (FCover) from the 30m resolution Landsat-8 surface reflectance data.

2.1. DEFINITION OF THE VARIABLES

LAI is defined as half the developed area of photosynthetically active elements of the vegetation per unit horizontal ground area. It determines the size of the interface for exchange of energy (including radiation) and mass between the canopy and the atmosphere. This is an intrinsic canopy primary variable that should not depend on observation conditions. LAI is strongly non-linearly related to reflectance. Therefore, its estimation from remote sensing observations will be scale dependent (Garrigues et al., 2006; Weiss et al., 2000). Note that vegetation LAI as estimated from remote sensing will include all the green contributors such as the understory when existing under forests canopies. However, except when using directional observations (Chen et al., 2005), LAI is not directly accessible from remote sensing observations due to the possible heterogeneity in leaf distribution within the canopy volume. Therefore, remote sensing observations are rather sensitive to the 'effective' leaf area index, i.e. the value that provides the same diffuse gap fraction while assuming a random distribution of leaves. The difference between the actual LAI and the effective LAI may be quantified by the clumping index (Chen et al., 2005) that roughly varies between 0.5 (very clumped canopies) and 1.0 (randomly distributed leaves). Note that similarly to the other variables, the retrieved LAI is mainly corresponding to the green elements: the correct term to be used would be GAI (Green Area Index) although we propose to still use LAI for the sake of simplicity.

FAPAR corresponds to the fraction of photosynthetically active radiation absorbed by the canopy. It is an essential climate variable in characterizing energy, mass and momentum exchanges between the canopy and the atmosphere and is an important input to a number of primary productivity models based on simple efficiency considerations (McCallum et al., 2009; Prince 1991). FAPAR depends on canopy structure, vegetation element optical properties and illumination conditions. Most of the primary productivity models using this efficiency concept are running at the daily time step. Consequently, the product definition should correspond to the daily integrated FAPAR value that can be approached by computation of the daily integrated FAPAR values for direct radiation as well as the FAPAR value computed for diffuse conditions. To be consistent with previous FAPAR products that are considering the instantaneous FAPAR value at the time of the satellite overpass assuming only direct radiation, a study investigated the differences between alternative FAPAR definitions (Baret et al., 2004). Results show that the instantaneous FAPAR value at 10:00 solar time is very close to the daily integrated value under only direct condition. To

keep the consistency with the FAPAR definition used in the CYCLOPES, MODIS and GEOV3 products, the instantaneous FAPAR value at 10:00 solar time under clear sky conditions was calculated (black-sky FAPAR). Moreover, to actual reflect the natural illumination condition (blue-sky), the FAPAR for the diffuse radiation was also provided assuming that the diffuse radiation is isotropic (white-sky FAPAR). Note that the FAPAR refers only to the green parts (leaf chlorophyll content higher than 15 ug cm^{-2}) of the canopy. FAPAR is relatively linearly related to the reflectance values, and is little sensitive to scaling issues (Weiss et al., 2000).

FCover corresponds to 1 minus the gap fraction for nadir direction. FCover is used to separate vegetation and soil in energy balance processes, including temperature and evapotranspiration. It is computed from the leaf area index and other canopy structural variables and does not depend on variables such as the geometry of illumination as compared to FAPAR. For this reason, it is a very good candidate for the replacement of classical vegetation indices for the monitoring of green vegetation. Because of its quasi-linear relationship with reflectance, FCover is only marginally scale dependent (Weiss et al., 2000).Note that similarly to LAI and FAPAR, only the green elements are considered.

2.2. BACKGROUND

The European Commission within Framework research Program and the GMES/Copernicus initiative supported the development of a series of biophysical products to be used within operational services.

The first series of products were derived from kilometric resolution sensors such as VEGETATION, recently completed by PROBA-V. The products included LAI, FAPAR and FCover. The first series of product called CYCLOPES was developed within the FP5 CYCLOPES project (Baret et al., 2007). It was tuned for the VEGETATION sensors. It was based on 2 steps. The first one was consisting in deriving dekadal top of canopy nadir like reflectances from the accumulation of observations within a fixed 30 days temporal compositing window. Then, a machine learning method (neural networks), trained over radiative transfer model simulations, was used to estimate the corresponding dekadal LAI, FAPAR and FCover products. The products were quite well received by the community and were characterized by a very good smoothness and good performances for the low to median amount of vegetation (Garrigues et al., 2008; Weiss et al., 2007). However, some limitations were identified, mainly coming by the pre-processing steps that create artefacts for the higher latitudes and a significant fraction of missing data due to the restricted length of the compositing window. In the meantime, the validation exercise was getting more mature, allowing inter-comparison of several available products. This was the basis of the following series of products developed within the FP7 GEOLAND2 project: the GEOV1 products were capitalizing on the previous development efforts (Baret et al., 2013). They are expected to take benefit from the advantages of the available products, while minimizing their

weaknesses. They are based on machine learning methods, but applied to the instantaneous daily observations available at the same time as the dekadal top of canopy reflectance values as derived from the CYCLOPES pre-processing steps. The radiative transfer simulations used in the CYCLOPES products were thus replaced by the actual products values derived from MODIS C5 and CYCLOPES V3.1. Significant improvements were observed as compared to MODISC5 and CYCLOPES products (Camacho et al., 2013). However, problems were remaining for the higher latitudes and a significant fraction of missing products was observed similarly to CYCLOPES. Within the end of GEOLAND2 and the start of the Copernicus Global Land service, the GEOV2 was developed to improve the performances of GEOV1 and provide near-real time products required by a number of applications. GEOV2 is still based on the training of a neural network using CYCLOPES and MODISC5 products (Verger et al., 2014). However, the compositing is now achieved on the biophysical products rather than on the surface reflectance as done in CYCLOPES and GEOV1. This improved the smoothness, reduced the artefacts in the higher latitudes and dramatically decreased the fraction of missing data. Emphasis was put here on the compositing step. Finally, GEOV2 was adapted to PROBA-V at 300 m resolution, resulting in GEOV3 that copes with the fact that no climatology was available at this resolution (the climatology being used in GEOV2 to fill gaps and smooth the temporal profiles).

The derivation of a product at the decametric resolution requires either the availability of an extended database of observations (or products as for the GEOVx series) or the use of radiative transfer model to simulate the products values as done in the CYCLOPES products. Because of the non availability of worldwide representative set of observations of LAI, FAPAR and FCover, it was decided to base the principle of the decametric products on radiative transfer model simulations. This was the basis of an algorithm proposed for Sentinel-2 (Baret et al., 2009; Verger et al., 2011a). The proposed algorithm is an adaptation of the previous algorithms tuned for Sentinel-2. This algorithm delivers instantaneous products corresponding to each Landsat-8 observations. It is the first step of the algorithm that will exploit jointly Landsat-8 and PROBA-V at 300m resolution to deliver near-real time products at decametric resolution.

2.3. OUTLINE OF THE ALGORITHM

The scheme of the algorithm is similar as the one proposed to Sentinel-2 products. For each product, one particular neural network is trained and used. It is composed of two steps (Figure 1):

- Training the neural network (NN)
- Operational use of the neural network
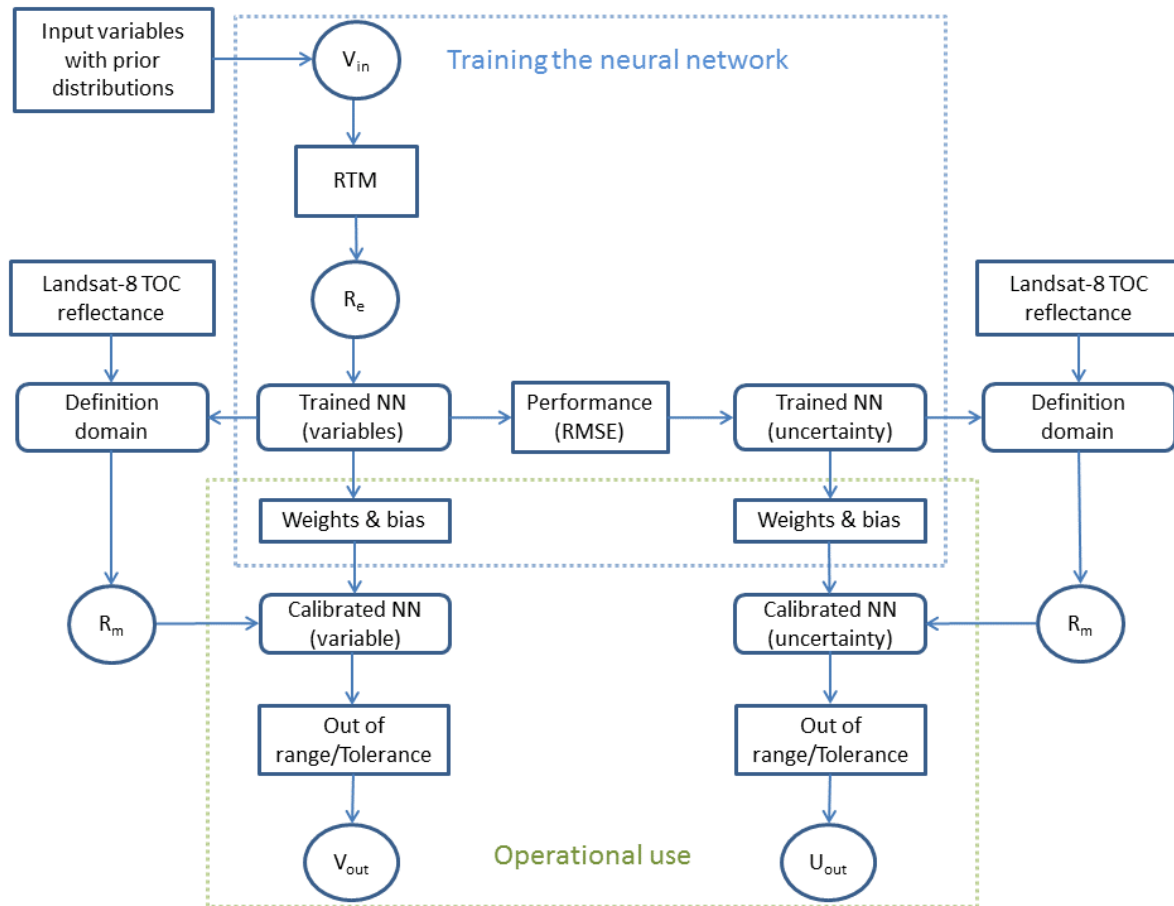
Figure 1. The flow chart of the main algorithm. V_{in} corresponds to the input variables for the model, R_e and R_m represent the estimated and measured top of canopy reflectance, respectively. V_{out} and U_{out} correspond to the output variable and associated uncertainty, respectively.

2.3.1. Training the neural network

- **Generate the training database.** It is based on the prior information on the distribution of the input variables to the models. The generated database should represent the actual distribution of variables.
- **Designing network architecture.** It consists in defining the optimal structure and possible transformations of the inputs and outputs.
- **Calibrating the network.** This last step corresponds to the actual training, i.e. adjusting the coefficients (synaptic weights and bias) that provide the best estimates of the biophysical variables.

2.3.2. Operational use of the neural network

Three networks are generated to produce the following variables: LAI, FAPAR and FCover. Another three networks are trained to generate the uncertainties associated to the

above variable estimates. Additional indicators are produced and are based on the following features:

- **Definition domain for the input data.** The actual Landsat-8 input reflectances should be consistent with those used in the simulated training data base. Therefore, when input reflectances are outside the convex hull defined by the simulated reflectance values of the training data base, i.e. the definition domain, then a specific 'input out of range' flag is raised.
- **Out of range indicators for the output variables.** This represents the output variables which should be within a predefined range determined by the simulated dataset and extended by given tolerance values, otherwise, a specific 'output out of range' flag is raised.
- **Quality flag.** This labels the quality of the data, including the pixels contaminated by cloud, out of range or water and snow.

2.4. THE RETRIEVAL METHODOLOGY

2.4.1. Input data

2.4.1.1. Top of Canopy reflectance

The top of canopy Landsat-8 reflectance data is generated based on the Multi-mission Atmospheric and Cloud Correction Software (MACCS) (Hagolle et al., 2008; Hagolle et al., 2010) algorithm, and are thus corrected from atmospheric, adjacency and terrain effects. A strict cloud mask is applied to the reflectance data to remove the pixels contaminated by clouds and clouds shadows. Reflectance should be expressed in terms of reflectance factor, mainly varying between 0 and 0.7 for most land surfaces outside the hot-spot or the specular directions and snow or ice cover. Four bands are used: B3 (green), B4 (red), B5 (NIR) and B6 (SWIR). These bands are selected to be consistent with PROBA-V spectral characteristics and the 300m biophysical products [ImagineS_RP2.1_ATBD-LAI300m]. And the green band is used as it is highly correlated with the vegetation responses. Figure 2 shows the relative spectral response on each Landsat-8 band used in this study and Figure 3 shows the corresponding bands of PROBA-V.
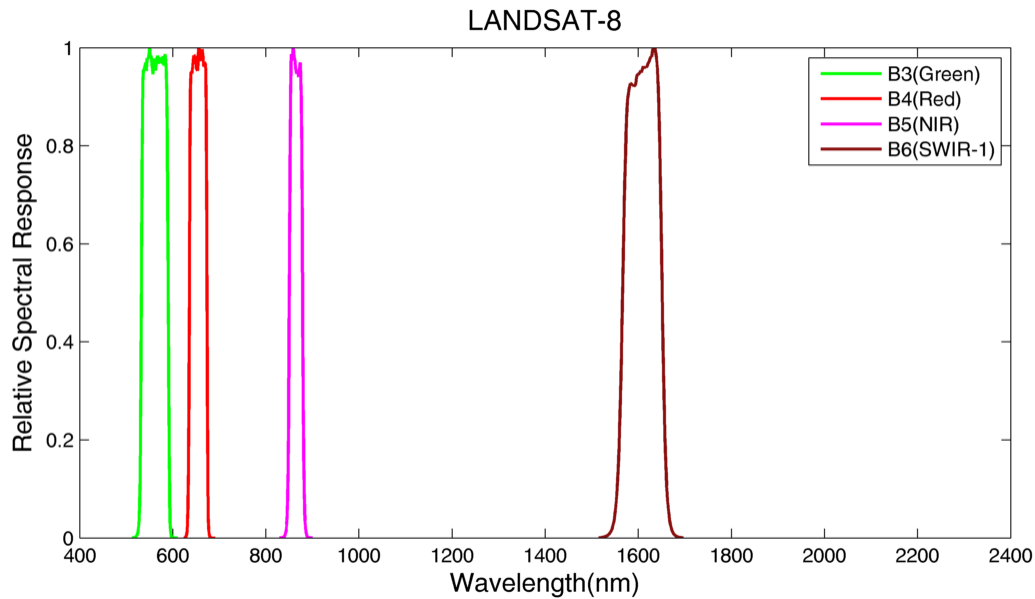
Figure 2. The relative spectral response of Landsat-8 bands used in this study.
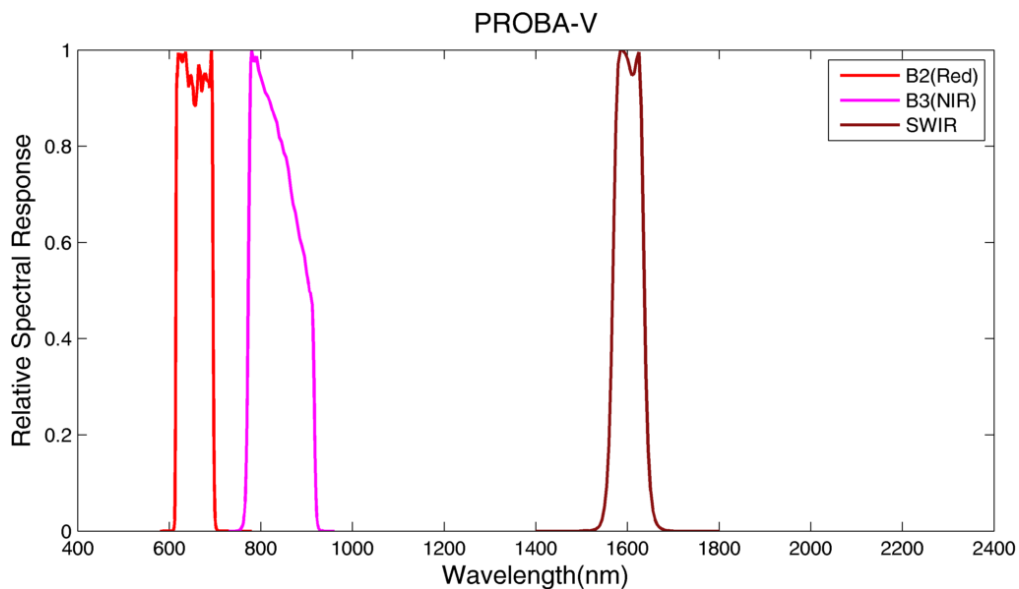

Figure 3. The relative spectral response of PROBA-V red, NIR and SWIR bands.

2.4.1.2. Geometry of acquisition

The geometry information is required as input to the neural network for the three variables LAI, FAPAR and FCover. It includes:

- The sun zenith angle (SZA)
- The sun azimuth angle (SAA)

The viewing geometry is assumed independent from the date and location. The view zenith angle (VZA) is set to nadir, and the view azimuth angle (VAA) is null.

2.4.2. The biophysical variables retrieval methodology

The retrieval methodology is composed of 2 main parts as shown in Figure 1: training the neural network and variables inversion. The general principles are summarized here. More details can be found in the ATBD [ImagineS_RP2.1_ATBD-LAI30m].

2.4.2.1. Reflectance models

The widely used PROSAIL radiative transfer model (Jacquemoud et al., 2009) was selected in this algorithm. The model couples the SAIL canopy reflectance model (Verhoef 1984) and the PROSPECT leaf optical model (Jacquemoud and Baret 1990). The SAIL model assumes the canopy as a turbid medium within which the leaves are randomly distributed. Canopy structure is characterized by LAI, the average leaf angle (ALA) assuming an ellipsoidal distribution (Campbell 1986), and a hot spot parameter (HOT) (Kuusk 1991). The PROSPECT model is widely used to simulate leaf optical properties through several structural and chemistry characteristics. In this study, the PROSPECT model with the updated absorption coefficients proposed by (Fourty and Baret 1997) was used. The soil reflectance data was simulated using five typical soil reflectance spectra multiplied by a brightness coefficient allowing to accurately represent a large soil dataset where soil types, roughness, moisture and observational geometry vary (Liu et al., 2003).

2.4.2.2. Generate the learning database

To generate a learning database that could best represent the possible types and states of actual canopies, the distribution law of the variable should be well considered (Baret et al., 2007; Verger et al., 2011b). Table 1 lists the range and distribution law for all variables of PROSAIL model. Some constraints on the co-distributions between variables were also introduced to restrict the space of canopy realization while keeping high degree of realism (Table 2). Note that the variables will be applied to all land cover types.

A full orthogonal experimental plan was adopted to randomly sample the variables according to the number of classes, variation range and distribution law defined above (Bacour et al., 2002). This sampling scheme could account for all the interactions between variables and generate a learning data base evenly but quasi-randomly populated. For each combination of variables in the learning data base, the top of canopy reflectance on each wavelength was simulated by running the PROSAIL model in a forward mode. Then the reflectance was spectrally integrated to represent actual Landsat-8 bands according to the spectral response function of the sensor (Figure 2). Instantaneous black-sky FAPAR, white-sky FAPAR at the satellite pass-by time (10:00 am for Landsat-8,) and FCover were

simulated by running the PROSAIL model in the forward mode using the same input variables.

Table 1. List of variables required to run PROSAIL model. The distribution law was described by using mode and standard deviation. Nb_Class represents the number of classes for each variable defined for the sampling purposes.

	Variable	Minimum	Maximum	Mode	Std	Nb_Class	Law
Canopy	LAI	0.0	15.0	2.0	2.0	6	Gauss
	ALA (°)	15	80	40	20	4	Gauss
	HOT	0.1	0.5	0.2	0.5	1	Gauss
Leaf	N	1.20	1.80	1.50	0.30	3	Gauss
	Cab ($\mu g.m^{-2}$)	20	90	45	30	4	Gauss
	Cdm ($g.m^{-2}$)	0.003	0.011	0.005	0.005	4	Gauss
	Cw_Rel	0.60	0.85	0.75	0.08	4	Uniform
	Cbp	0.00	2.00	0.00	0.30	3	Gauss
Soil	Bs	0.50	3.50	1.20	2.00	4	Gauss

Table 2. The co-distribution laws for PROSAIL input variables with LAI.

	Variable	Co-distribution	$V_{min}(0)$	$V_{max}(0)$	$V_{min}(LAI_{max})$	$V_{max}(LAI_{max})$
Canopy	ALA (°)	Yes	30	80	55	65
	HOT	Yes	0.1	0.5	0.1	0.5
Leaf	N	No	1.2	2.2	1.30	1.8
	Cab	Yes	20	90	45	90
	Cdm	Yes	0.003	0.011	0.0050	0.0110
	Cw_Rel	Yes	0.6	0.85	0.70	0.80
	Cbp	Yes	0.00	2.00	0.00	0.20
Soil	Bs	No	0.5	3.50	0.50	1.20

The radiative transfer model introduces uncertainties to the simulated reflectance due to its adequacy to represent the actual canopy architecture. This mainly results in structured errors. The accuracy of actual measured top of canopy reflectance is also inevitably influenced by several possible factors, including the instrumental noises, radiometric calibration, atmospheric correction and cloud or cloud shadow contaminations. These factors will lead to multiplicative or additive uncertainties to the measured reflectance (Verger et al., 2011b). To get a more realistic canopy reflectance closer to the actual measurements, an uncertainty model was used to describe the additive and multiplicative uncertainties based on a white Gaussian noise:

$$R^*(\lambda) = R(\lambda) \ (1+(MD(\lambda)+MI)/100)+AD(\lambda)+AI \qquad (1)$$

where $R(\lambda)$ is the raw simulated reflectance, $R^*(\lambda)$ is the reflectance contaminated with noise, MD is the multiplicative wavelength dependent noise, MI is the multiplicative

wavelength independent noise, AD is the additive wavelength dependent noise, and AI is the additive wavelength independent noise. In this study, the MD, MI, AD and AI was fixed to 0.02, 0.02, 0.01, and 0.01 for all bands of each sensor.

A total of 55296 cases were simulated with input canopy variables and output reflectance, FAPAR and FCover. The database was divided into two parts: two thirds of the simulations were randomly selected to train the neural network, and the remaining one third of the simulations was used for the hyper-specialization control and the theoretical performances evaluations.

2.4.2.3. *Train the neural network*

The dedicated back-propagation artificial neural network (Rummelhart et al., 1986) was used in this study. The network is made of one input layer composed of the normalized input data, one hidden layer composed of 5 neurons with tangent sigmoid transfer functions and one output layer with a linear transfer function. The input layer of the network corresponds to the surface reflectance for each band and the geometrical configurations; the outputs are LAI, black-sky FAPAR, white-sky FAPAR and FCover. The normalization applied to the input and output variables is expected to increase the performances of the Levenberg-Marquardt minimization algorithm (Ngia and Sjoberg 2000) used in the training process. For each output variable, five networks were trained in parallel with different initial solutions. The best one is selected based on the smallest RMSE between the outputs and the 'true' biophysical variables computed over the validation data set. The theoretical performances of the 5 neural networks were very close and the performances obtained with the best neural network for each variable demonstrate the success of the training process (Figure 4). Then, a specific neural network was trained for each product to relate the estimated uncertainties of the neural network to the input reflectance and observation geometry values.
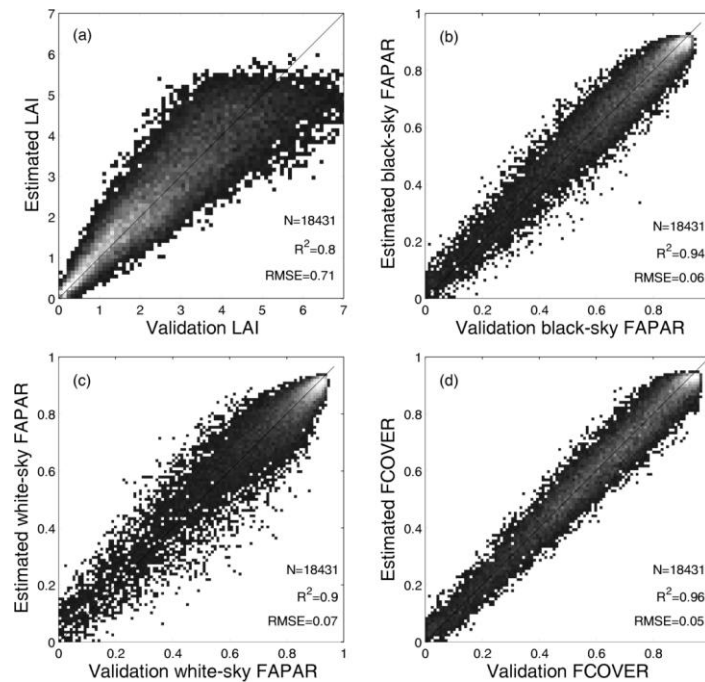
Figure 4. The theoretical performances of the neural network for (a) **LAI,** (b) **black-sky FAPAR,** (c) **white-sky FAPAR, and** (d) **FCover.**

2.4.2.4. Inversion

In the actual inversion process, two practical strategies were proposed to control the quality of the inversed products. First, the input reflectance data should be consistent with those used in the learning data base. A definition domain was therefore defined by the co-distribution of the simulated reflectance on each band. Figure 5 shows the definition domain for four Landsat-8 bands used in this study. Pixels with reflectance values outside of the definition domain will be reported as 'input out of range'. The solar zenith angle for each image was also calculated. Only the images with solar zenith angle smaller than 65° will be used in further analysis. Second, the output variables should be within a predefined range determined by the simulated dataset and extended by a small tolerance interval (Table 3), otherwise, an 'output out of range' flag will be raised for the pixel. For each measurement, the inversion process was run to obtain LAI, black-sky FAPAR, white-sky FAPAR and FCover, and corresponding uncertainties.
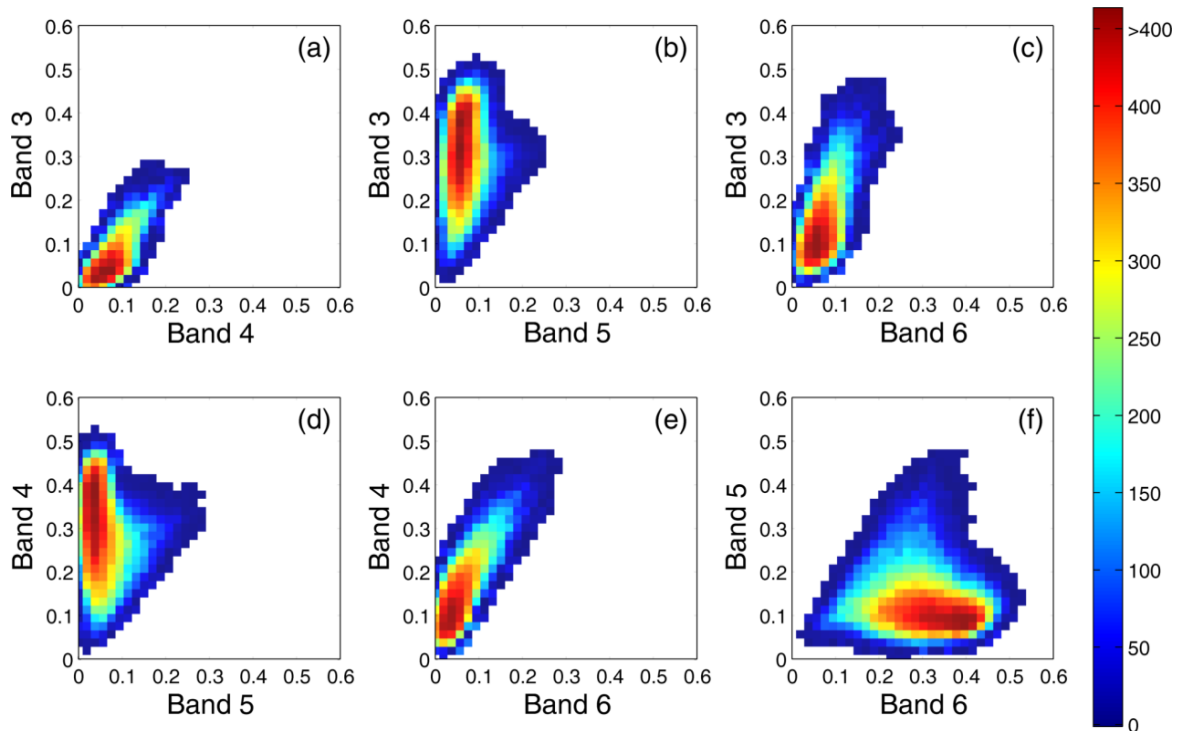
Figure 5. The definition domain (colorful region) of the simulated TOC reflectance on four Landsat-8 bands. The color indicates the number of cases simulated in the neural networks learning database.

Table 3. The minimum, maximum range and tolerance for each output product.

	Minimum	Maximum	Tolerance
LAI	0	7	±0.2
Black-sky FAPAR	0	0.94	±0.05
White-sky FAPAR	0	0.94	±0.05
FCover	0	1	±0.05

2.4.3. The quality indicators

The quality indicators include two parts: the quality assessment indicators and the quality flag.

2.4.3.1. Quality assessment indicators

The quality assessment indicators correspond to the products uncertainty. Based on the training dataset and validation dataset, the theoretical performances of the algorithm can be calculated from the RMSE between the estimated and actual biophysical values. A specific

neural network is then trained for each product to relate the estimated uncertainties to the input reflectance and observation geometry values.

2.4.3.2. *Quality flags*

The quality flags indicate the pixels with low quality due to cloud or cloud shadow contamination, water or snow, input reflectance out of definition domain or output variables out of range. The details are given in Table 7.

2.5. LIMITATIONS OF THE PRODUCT

The derived Landsat-8 LAI is close to field measured effective LAI because the foliage clumping is not fully accounted. This may lead to an underestimation of the foliage amount for the aggregated vegetation such as forest. This underestimation will be severely for highly clumped coniferous forests and evergreen forests. Further work will be done to consider the clumping effects at this decametric scale.

3. PRODUCT DESCRIPTION

The high resolution Landsat-8 LAI, FAPAR, FCover product files are named as the following:

IMAGINES_<Acronym>_<YYYYMMDD>_<AREA>_<PathRow>_<SENSOR>

where

- <Acronym> is the short name of each product i.e. LAI, BS-FAPAR (Black-sky FAPAR), WS-FAPAR (white-sky FAPAR) or FCover.

- <YYYYMMDD> provides the temporal information of the file. YYYY, MM and DD denote the year, the month and the day, respectively.

- <AREA> provides the name of the site (Table 4).

- <PathRow> provides the path and row number of the original Landsat-8 scene. If the path and row are less than 3 digits, they are completed by '0' in the beginning. This information is provided to clarify the images covered by more than one scene on each date.

- <SENSOR> gives the name of the sensor used to retrieve the products, so Landsat-8.

3.1. FILE FORMAT

The Landsat-8 products are distributed for 8 IMAGINES demonstration site (Table 4). For each site, the zip archive contains 3 multi-band GEOTIFF format files containing the following layers:

- LAI (or BS-FAPAR, or WS-FAPAR or FCover)

- Uncertainty of LAI (or of BS-FAPAR, or of WS-FAPAR or of FCover)

- Quality flags for LAI (or for BS-FAPAR, or for WS-FAPAR or for FCover)

The zip archive contains also PNG images of the variables (LAI, or BS-FAPAR, WS-FAPAR or FCover).

Table 4. Information of 8 IMAGINES demonstration sites.

Area	Location	Coordinate	Period	Path/row	Image numbers
25DEMAYO	25 de Mayo, Pampa, Argentina	37° 54' S 67° 44' W	01/11/2013 - 04/11/2014	230, 86	17
ALBUFERA	La Albufera, Spain	39° 16' N 0° 19' W	1/11/2013 - 26/10/2014	199, 30; 198, 30	22
BARRAX	Las tiesas Farm, Barrax, Spain	39° 02' N 2° 04' W	30/10/2013 - 26/10/2014	199, 33; 200, 33	24
OTTAWA	Greenbelt Farm, Ottawa, Canada	45° 18' N 75° 45' W	21/04/2013 - 09/11/2014	15, 29; 16, 28	24
PSHENICHNE	Pshenichne, Ukraine	50° 4' N 30° 6' E	16/04/2013 - 04/11/2014	181, 25; 182, 25	39
ROSASCO	Rosasco, Milan, Italy	45° 15' N 8° 33' E	05/11/2013 - 08/11/2014	194, 28	13
SOUTHWEST	South-west, France	43° 29' N 1° 16' E	14/04/2013 - 20/11/2014	198, 30; 199, 30	46
TANA	Upper Tana Basin, Kenya	0° 55' N 36° 47' E	01/07/2013 - 11/12/2014	169, 59; 168, 60; 168, 59	92

3.2. PRODUCT CONTENT

The physical range of LAI, FAPAR, FCover are given in Table 5. The physical values are retrieved by:

$$PhyVal = DN / ScalingFactor + Offset$$

where the scaling factor and the offset are given in Table 5.

Table 5. Range of values and scaling factors of LAI, FAPAR and FCover.

Variables	Minimum physical value	Maximum physical value	Maximum DN value	Scaling factor	Offset	Invalid values
LAI	0	7	210	30	0	255
Black-sky FAPAR	0	0.94	235	250	0	255
White-sky FAPAR	0	0.94	235	250	0	255
FCover	0	1	250	250	0	255

The physical range, the scaling factors and offset of the uncertainty layers are given in Table 6.

Table 6. Range of values and scaling factors of uncertainties of LAI, FAPAR and FCover.

Uncertainties of variables	Minimum physical value	Maximum physical value	Maximum DN value	Scaling factor	Offset	Invalid values
LAI	0	1.25	250	200	0	255
Black-sky FAPAR	0	0.2	40	200	0	255
White-sky FAPAR	0	0.2	40	200	0	255
FCover	0	0.2	40	200	0	255

The quality flag layer for each variable is described in Table 7.

Table 7. Quality flag of Landsat-8 LAI, FAPAR and FCover products.

Bit	Qualitative quality indicator	Meaning
1	Cloud or cloud shadow	Bit1 = 0: cloud or cloud shadow Bit1 = 1: no cloud
2	Land / Water(snow)	Bit2 = 0: Water or snow (heritage from Landsat8 surface reflectance data) Bit2 = 1: Land without water and snow
3	Input out of definition domain	Bit3 = 0: input surface reflectance out of the definition domain Bit3 = 1: input surface reflectance within the definition domain
4	Output out of range	Bit4 = 0: output LAI (or BS-FAPAR, or WS-FAPAR, or FCover) out of the range Bit4 = 1: output LAI (or BS-FAPAR, or WS-FAPAR, or FCover) within the range

The quality layer is also shown in int16 format. For restrict usage, value of '15' indicate good quality pixels, that no cloud, no snow, input and output all within the range.

3.3. PRODUCT CHARACTERISTICS

3.3.1. Projection and Grid Information

The products are provided in the UTM projection, in the datum of WGS-84. This projection uses different zones for separate sites. The resolution of the grid is 30m, as the original Landsat-8 resolution. Each site covers a region centered at the site coordinate (Table 4) and is located by the upper left corner pixel. The projection information for each site is shown in Table 8.

Table 8. The projection information and spatial size of each site.

AREA	Projection	Datum	Zone	N / S	Row	Column
25DEMAYO	UTM	WGS-84	19	S	2000	2000
ALBUFERA	UTM	WGS-84	30	N	2000	2000
BARRAX	UTM	WGS-84	30	N	2000	2000
OTTAWA	UTM	WGS-84	18	N	2000	2000
PSHENICHNE	UTM	WGS-84	36	N	2000	2000
ROSASCO	UTM	WGS-84	32	N	2000	2000
SOUTHWEST	UTM	WGS-84	31	N	2000	2000
TANA	UTM	WGS-84	37	N	1165	720

3.3.2. Spatial information

As shown in Table 8, the general spatial size is 60 * 60 km^2 for European sites, and 34.95 * 21.6 km^2 for Kenya site. On Kenya site, the study area was overlapped by three scenes. Thus, the overlapped subset was extracted to keep the information from all scenes.

3.3.3. Temporal Information

The products are provided on actual Landsat-8 measurement dates, given in the name of the file. The period covered by the product time series for each site is shown in Table 4.

3.4. DATA POLICIES

Any use of the IMAGINES Landsat-8 LAI, FAPAR, FCover products implies the obligation to include in any publication or communication using these products the following citation:

"*The research leading to these products has received funding from the European Community's Seventh Framework Program (FP7/2007-2013) ImagineS project under the Grant Agreement N°311766. These products are the property of INRA under copyright ImagineS. They are generated from the Landsat-8 surface reflectance data processed and distributed by CESBIO and USGS (Kenya site).*"

The users accepts to inform the ImagineS project of their publications through the following address: rl@hygeos.com

3.5. ACCESS AND CONTACT

The Landsat-8 LAI, FAPAR, FCover product are available through the IMAGINES website (http://fp7-imagines.eu/pages/services-and-products/high-resolution-biophysical-products.php). Connection information to access the products are given after registration.

Scientific contact: Institut National de la Recherche Agronomique (INRA), France

Email address: frederic.baret@avignon.inra.fr

4. QUALITY ASSESSMENT

The quality of the products was assessed by comparing with the field measurements directly. Several field measurements campaigns were conducted on the sample sites to provide ground LAI, FAPAR and FCover data for the direct validation of remote sensing products (http://fp7-imagines.eu/pages/services-and-products/ground-data.php). The general strategy of the field measurements is based on the guidelines proposed by the CEOS LPV group (Morisette et al., 2006) and the VALERI project (http://w3.avignon.inra.fr/valeri/). ESU level LAI, daily integrated black-sky FAPAR, daily integrated white-sky FAPAR and FCover were measured using digital hemispherical cameras and calculated using CAN_EYE (Weiss and Baret 2010). These ESU measurements were then up-scaled to high spatial resolution ground-based map by using empirical transfer functions. More details about the ground measurement data collection and ground map generation on each site can be found in (Latorre et al., 2014a; Latorre et al., 2014b; Latorre et al., 2014c; Latorre et al., 2014d; Sánchez et al., 2014; Sendra et al., 2014)

For this quality assessment, we use the ground measurements data available on six sites, including SOUTHWEST (France), ALBUFERA (Spain), ROSASCO (Italy), PSHENICHNE (Ukraine), 25DEMAYO (Argentina) and BARRAX (Spain). The quality of Landsat-8 biophysical products is firstly assessed by comparing all ESU measurements over six sites to provide an overview (Section 4.1). Then, validation is conducted per site in two steps: the first step compares the Landsat-8 products with the raw ESU measurements; the second step compares theLandsat-8 products with the high resolution ground-based map (5km x 5km). For that, only the best quality pixels of the ground maps (QFlag=1) and of Landsat-8 products (QF=15) are used.

4.1. ALL SITES

Figure 6 shows that the Landsat-8 products have good correlation with the field measurements, except for some scatterings. These scatters will be analyzed following for each site.
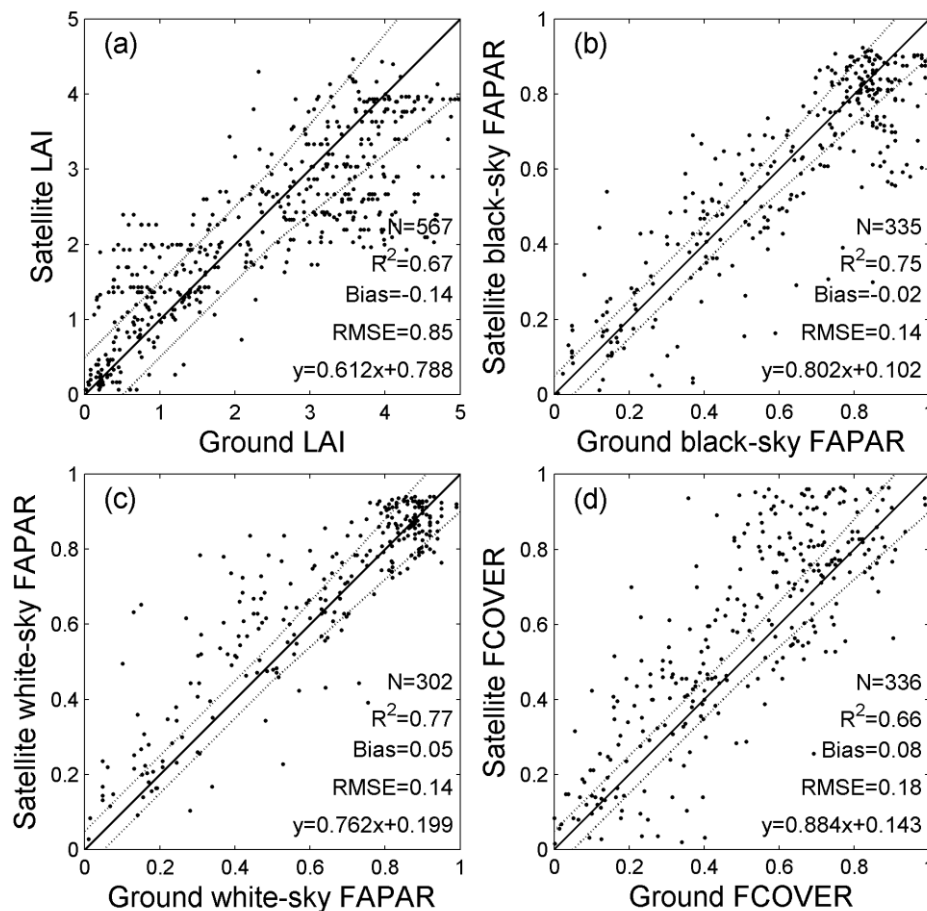
Figure 6. Direct validation of (a) LAI, (b) black-sky FAPAR, (c) white-sky FAPAR and (d) FCover Landsat-8 products with the ground measurements over 6 sites, including SOUTHWEST, ALBUFERA, ROSASCO, PSHENICHNE, 25DEMAYO and BARRAX. The dashed lines represent the GCOS requirements boundary.

4.2. SOUTHWEST

Ground measurements data over three main land cover types (wheat, maize and sunflower) were collected from 17th of April to 26th of June in 2013 using the downward-looking digital hemispherical cameras (Sánchez et al., 2014). Since the field measurements dates were not exactly on the same dates of Landsat-8 observations, the ground data were linearly interpolated firstly. The ground data on Landsat-8 observations dates were extracted and compared with Landsat-8 biophysical products. Results show that the biogeophysical products are correlated well with the field measurements (R^2>0.79), although with a slight bias of 0.07 for LAI, 0.05 for FAPAR (black-sky FAPAR and white-sky FAPAR) and 0.09 for FCover (Figure 7). LAI products have the best performance, with 77% of pixels within the GCOS (GCOS 2011) boundaries (max(0.5, 20%)). For FAPAR, 50% of the black-sky FAPAR and 52% of white-sky FAPAR meet the GCOS requirements (max (0.05, 10%)). For FCover,

using the same requirements as for FAPAR, only 32% of pixels are within the GCOS range. Note that these percentage values are only calculated from the validation pixels, not the whole image. More information about the validation could be found in (Li et al., 2015).
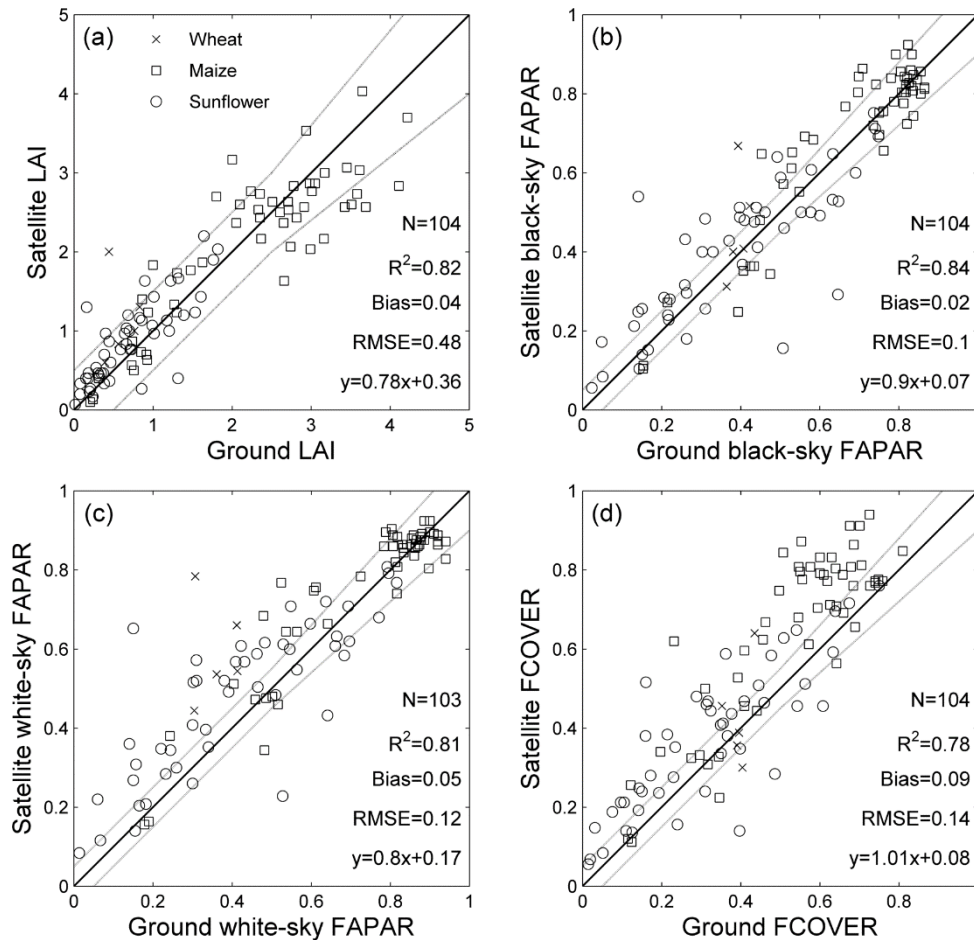

Figure 7. Direct validation of (a) LAI, (b) black-sky FAPAR, (c) white-sky FAPAR and (d) FCover Landsat-8 products with all ground measurements over three biomes from 17th of April to 26th of June in 2013. The dashed lines represent the GCOS requirements boundary.

Three high spatial resolution ground-based maps were generated from field measurements. For each ground map, closest Landsat-8 biophysical products were found and used for comparison. Two validation sites are identified in this region (Sánchez et al., 2014) and both are used in the validation. Figure 8 shows that the Landsat-8 products generally correspond well with the field measurements on all validation dates. On the first date pair (ground data on 22nd of June and satellite data on 26th of June), Landsat-8 black-sky FAPAR and FCover show an underestimation at large values. This may be because of the overestimation of transfer function estimates at very large values (>0.8, Figure 12 in Sánchez et al., 2014).
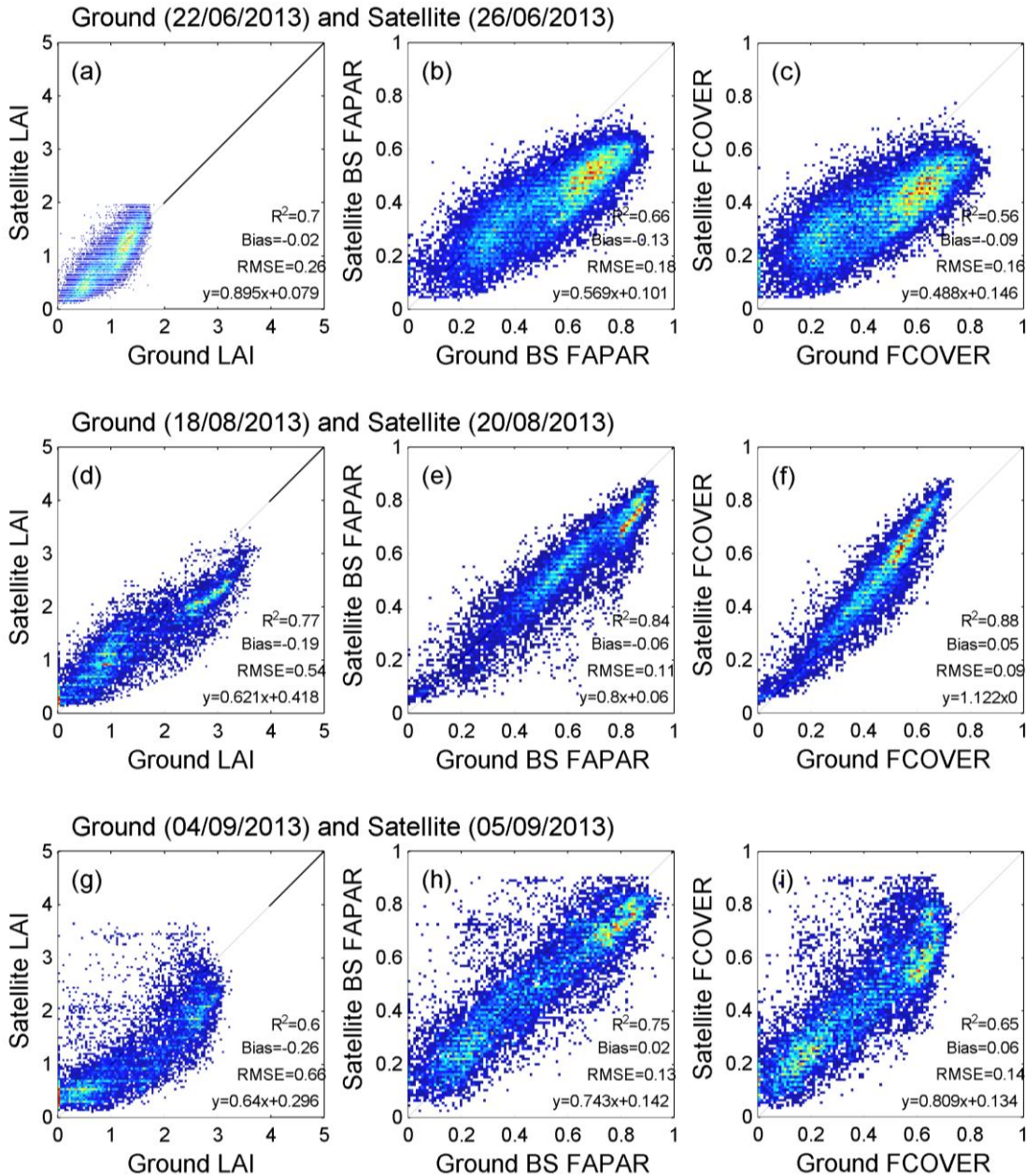
Figure 8. Direct validation of (a) LAI, (b) black-sky FAPAR, and (c) FCover Landsat-8 products with high spatial resolution ground measurements map on three dates pairs over the 2 validation sites of the SOUTHWEST region.

4.3. ALBUFERA

Nine field campaigns of LAI, FAPAR and FCover measurements were conducted between 17th of June and 22nd of August. Several instruments are used, including downward-looking digital hemispherical cameras, LAI-2200, AccuPAR and PocketLAI (Sendra et al., 2014). All field measurements are used to compare with the closest Landsat-8 product. More

ground effective LAI measurements are available than the other variables. On the ESU level, results show that the derived products generally correspond well with the ground measurements for LAI, black-sky FAPAR and FCOVER (R^2>0.6, Figure 9). But obvious biases are observed when comparing ground data on 17th of June and satellite data on 20th of June. It may be partly due to the quick growth of the canopy, leading to the bias within three days. It may also be partly due to the low representativeness of the learning database for biomes with water flooded or saturated soil background. This site is dominated by rice paddy fields, which own the combination of soil and water during most of the growing season. This problem will be solved by enlarging the representativeness of the background learning database in the next step or using specific learning database for this special biome.
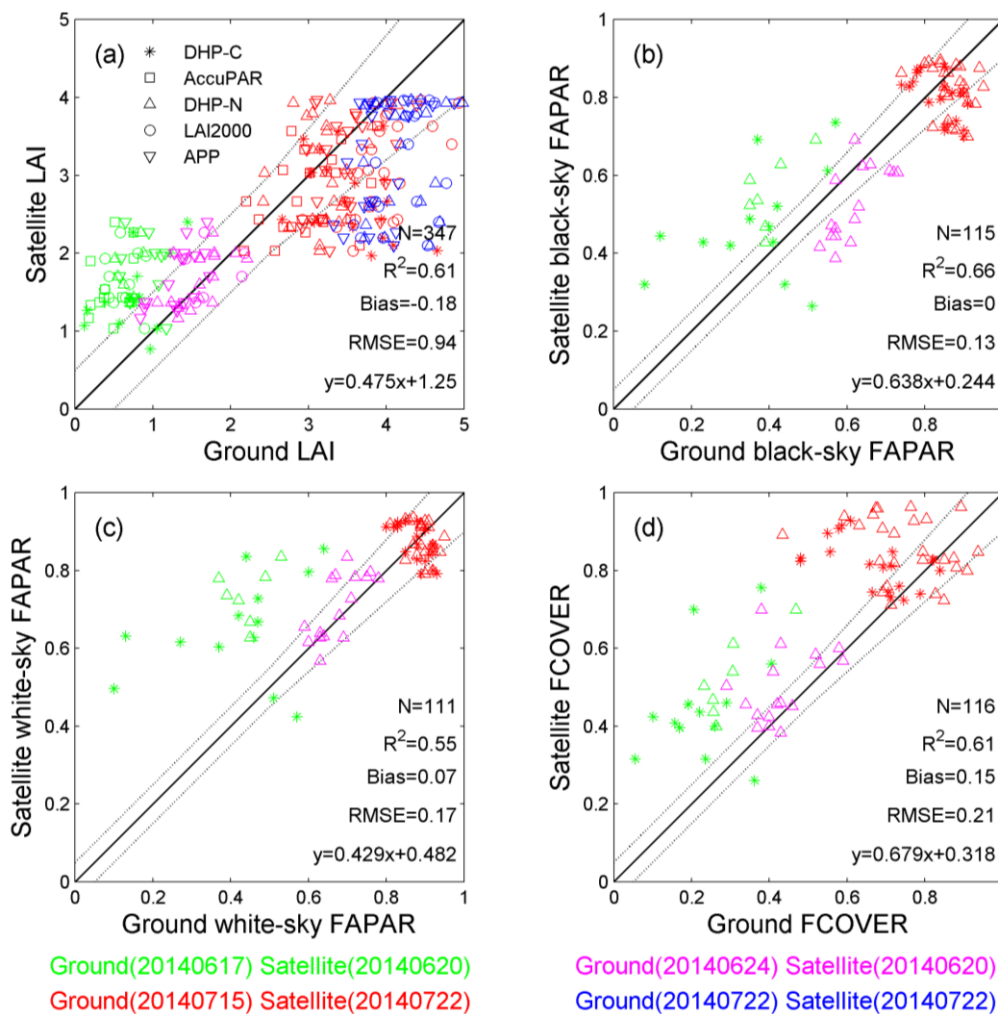

Figure 9. Direct validation of (a) LAI, (b) black-sky FAPAR, (c) white-sky FAPAR and (d) FCover Landsat-8 products with the ground measurements on multiple dates over ALBUFERA site. DHP-C represents the ground values obtained by Canon DHP, and DHP-N represents that by Nikon DHP. APP represents LAI measured using PocketLAI instrument.

Five high-spatial resolution ground maps in the size of 5km by 5km are available, and three (17th of June, 24th of June and 15th of July) are used to compare with the Landsat-8 products according to the availability of valid pixels on Landsat-8 images. Comparing with all high-spatial resolution ground maps, the Landsat-8 products have a good performance (Figure 10). But an overestimation of Landsat-8 products is observed for the first date pair (ground data on 17th of June and Landsat-8 products on 20th of June), which has same reasons as Figure 9. On the first and second date pairs, Landsat-8 FCover is larger than the field measurements (bias=0.2), which is also shown in Figure 9.
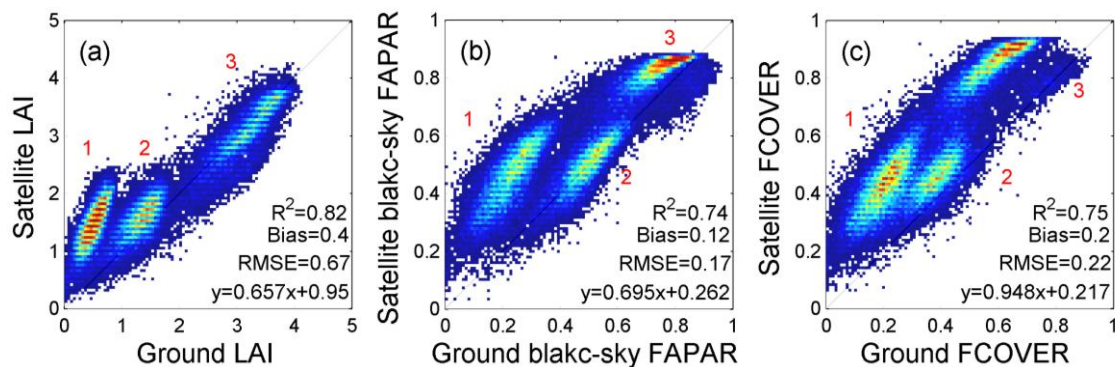

Figure 10. Direct validation of (a) LAI, (b) black-sky FAPAR, and (c) FCover Landsat-8 products with high spatial resolution ground measurements map over ALBUFERA site on three pairs of dates: '1' represents the pair of ground data on 17/06/2014 and Landsat-8 products on 20/06/2014; '2' represents the pair of ground data on 24/06/2014 and Landsat-8 products on 20/06/2014; '3' represents the pair of ground data on 15/07/2014 and Landsat-8 products on 22/07/2014.

4.4. ROSASCO

Ground measurements data on the ROSASCO site were collected on 3rd and 4th July 2014 using the downward-looking digital hemispherical cameras (Latorre et al., 2014a). The dominated crop is rice, corn and soybean. Results show that Landsat-8 products have a good correspondence with raw field measurements on maize and soybean fields (Figure 11). But they show an obvious underestimation on rice fields, which is mainly due to the low representative of learning database for biomes with flooded or saturated soil background.
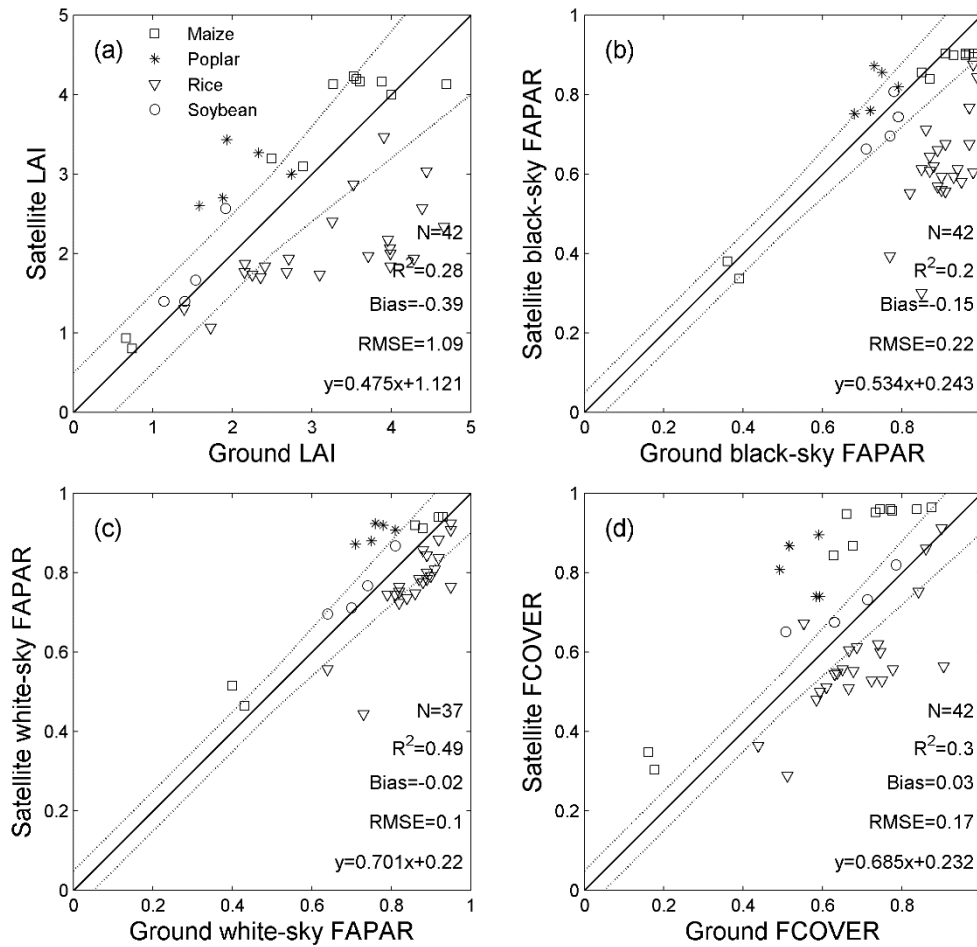
Figure 11. Direct validation of (a) LAI, (b) black-sky FAPAR, (c) white-sky FAPAR and (d) FCover Landsat-8 products (03/07/2014) and the ground measurements (03/07/2014) on ROSASCO site.
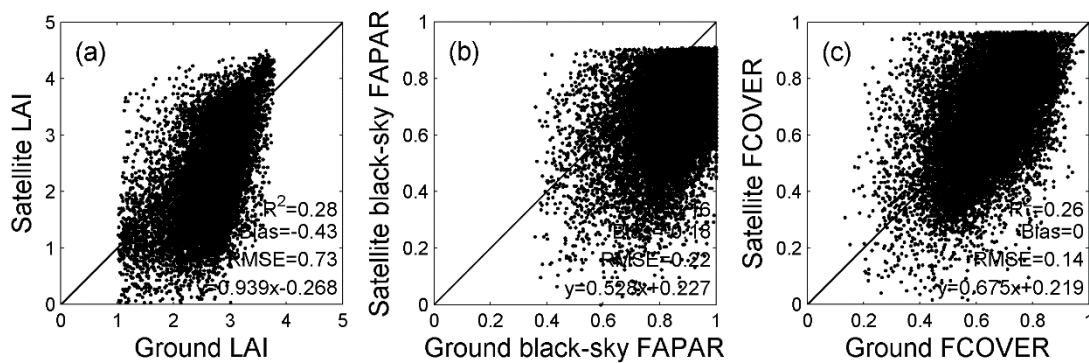

Figure 12. Direct validation of (a) LAI, (b) black-sky FAPAR, and (c) FCover Landsat-8 products (03/07/2014) with high spatial resolution ground measurements map (03/07/2014) on ROSASCO site.

Figure 12 shows that the Landsat-8 products are not correlated well with the ground map. It is partly due to the low representativeness of the training database for paddy rice (Figure 11), and partly due to the large dispersion of the transfer function on this site (Figure 19 in Latorre et al., 2014).

4.5. PSHENICHNE

Two ground measurements datasets on the PSHENICHNE site were collected on 12th of June and on 31st of July 2014 using the downward-looking digital hemispherical cameras (Latorre et al., 2014d). The dominated crop is maize sunflower, barley and winter wheat. Ground data on 31st of July are used according to the availability of Landsat-8 data. On the ESU level, results show the Landsat-8 products correspond very well with the ground data (R^2>0.8, Figure 13). 56% of Landsat-8 LAI are within the GCOS requirement (max (0.5, 20%)), and 52% of black-sky and 40% of FCover could satisfy the GCOS requirement (max (0.05, 10%)). Landsat-8 products on winter wheat and barley have obvious underestimation on small values, which may be due to influences of senescent canopies. On 31st of July, the winter wheat and barley have entered the end of the growing stage and have a large part of senescent leaves (decreased LAI from 12th of June to 31st of July in Figure 8 of Latorre et al., 2014d). The Landsat-8 observations correspond to green leaves, while the field measurements may include some yellow leaves due to the difficulty to separate green leaves from senescent leaves. This may lead to the underestimation of Landsat-8 products on barley and winter wheat crops.
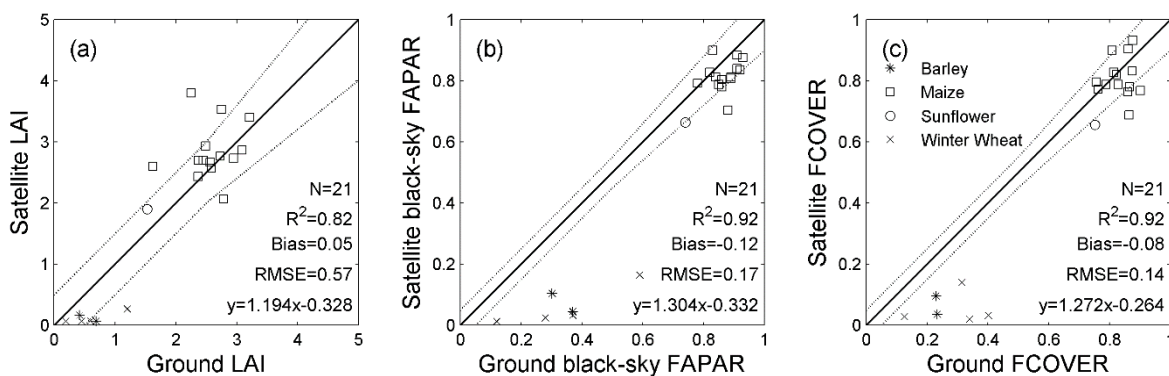

Figure 13. Direct validation of (a) LAI, (b) black-sky FAPAR, and (c) FCover Landsat-8 products (31/07/2014) with the ground measurements (31/07/2014) on PSHENICHNE site. The dashed lines represent the GCOS requirements boundary.

On the ground map level, the Landsat-8 products correspond well with the ground maps values (R^2>0.8, Figure 14). But some biases are shown for all variables, which are similar to those in Figure 13.
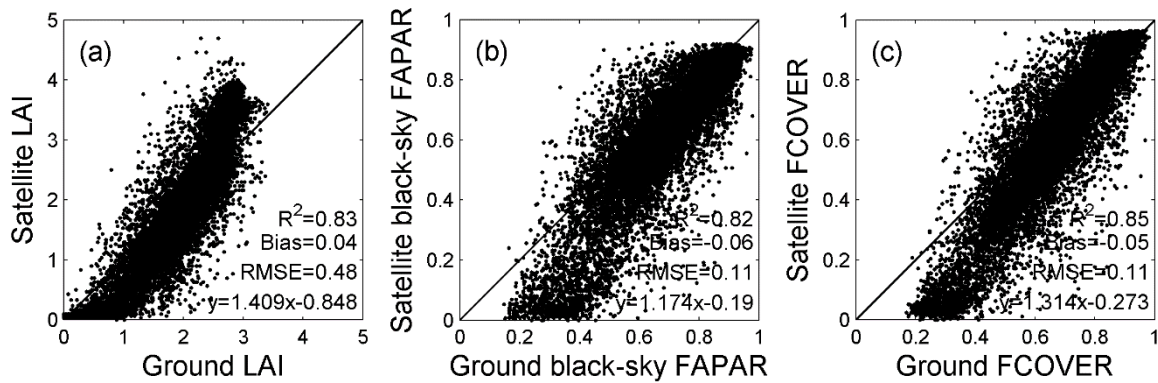

Figure 14. Direct validation of (a) LAI, (b) black-sky FAPAR, and (c) FCover products derived from Landsat-8 sensor (31/07/2014) with high spatial resolution ground measurements map (31/07/2014) on PSHENICHNE site.

4.6. 25DEMAYO

Ground measurements data on the 25 de Mayo site were collected from 7th to 9th of February 2014 using the downward-looking digital hemispherical cameras (Latorre et al., 2014c). The Landsat-8 products on 5th of February are selected by assuming that the vegetation status remains stable within 4 days. Results show the Landsat-8 products correspond very well with the ground data (R^2>0.8, Figure 15). 88.1% of Landsat-8 LAI are within the GCOS requirement (max (0.5, 20%)), and more than half of black-sky and whit-sky FAPAR could satisfy the GCOS requirement (max (0.05, 10%)). For FCover, using the same requirements as for FAPAR, only 28.6% of validation pixels are within the GCOS range.
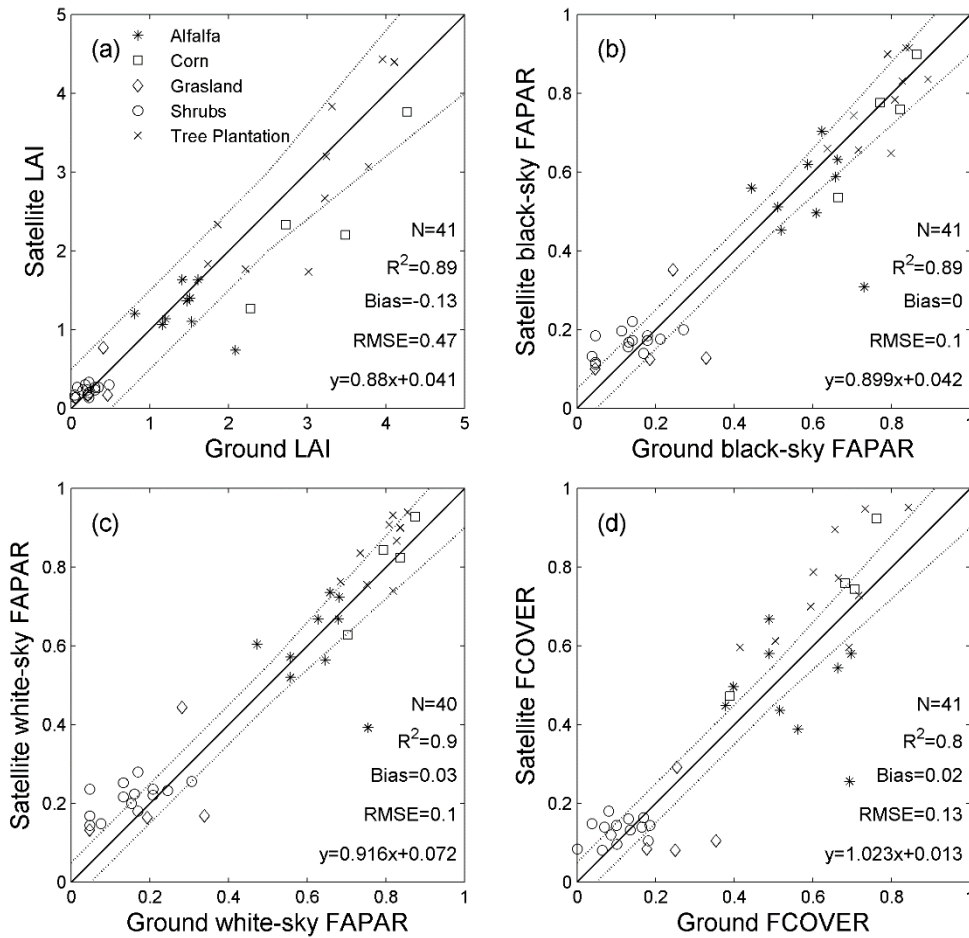
Figure 15. Direct validation of (a) LAI, (b) black-sky FAPAR, (c) white-sky FAPAR and (d) FCover Landsat-8 products (05/02/2014) with the ground measurements (09/02/2014) on 25DEMAYO site. The dashed lines represent the GCOS requirements boundary.
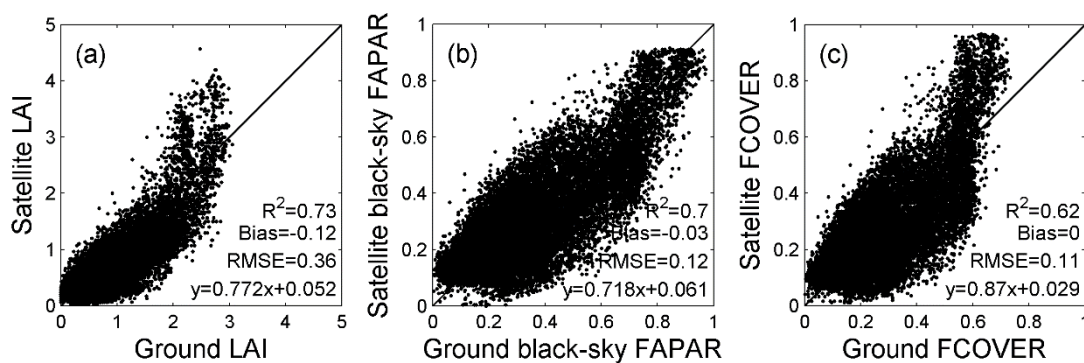

Figure 16. Direct validation of (a) LAI, (b) black-sky FAPAR, and (c) FCover Landsat-8 products (05/02/2014) with high spatial resolution ground measurements map (09/02/2014) on 25DEMAYO site.

Figure 16 shows the regressions between Landsat-8 products and high spatial resolution field maps. A good correspondence ($R^2>0.7$) is observed for LAI and black-sky FAPAR,

although Landsat-8 products have an overestimation on large values of LAI. For FCover, the overestimation of Landsat-8 FCover on point validation (Figure 15) also shows on the ground map validation (Figure 16 c).

4.7. BARRAX

Ground measurements data on the BARRAX site were collected from 29th to 30th of May 2014 using the downward-looking digital hemispherical cameras (Latorre et al., 2014b). The Landsat-8 products on 26th of May are selected by assuming that the vegetation status remains stable within 3 days. Results show the Landsat-8 products correspond very well with the ESU ground data (R^2>0.8, Figure 17). Most of Landsat-8 LAI and FAPAR validation pixels could satisfy the GCOS requirement (LAI: max (0.5, 20%)) and FAPAR: max (0.05, 10%)). For FCover, obvious overestimation is observed for Landsat-8 data, especially on wheat sites. The overestimation may be due to the different foot print of FCover between satellite products and field measurements. The satellite FCover corresponds strictly to the nadir direction, while the ground FCover is estimated within a +-10° field of view. It is therefore dependent on the sampling strategy (center of row or on the canopy). Further, the size of the footprint for FCover may be too low using 12 images to represent a Landsat pixel (footprint is around 1.3m² with 12 images acquired at 1m height)
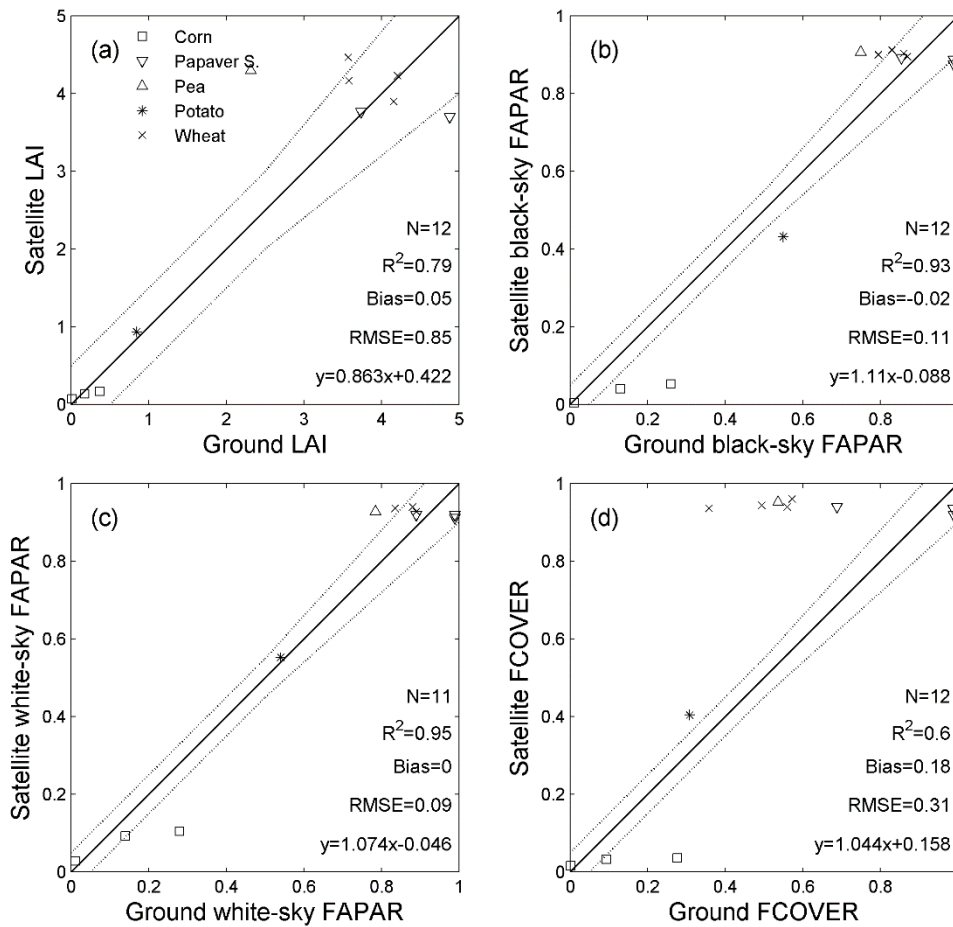
Figure 17. Direct validation of (a) LAI, (b) black-sky FAPAR, (c) white-sky FAPAR and (d) FCover Landsat-8 products (26/05/2014) with the ground measurements (29/05/2014) on BARRAX site. The dashed lines represent the GCOS requirements boundary.
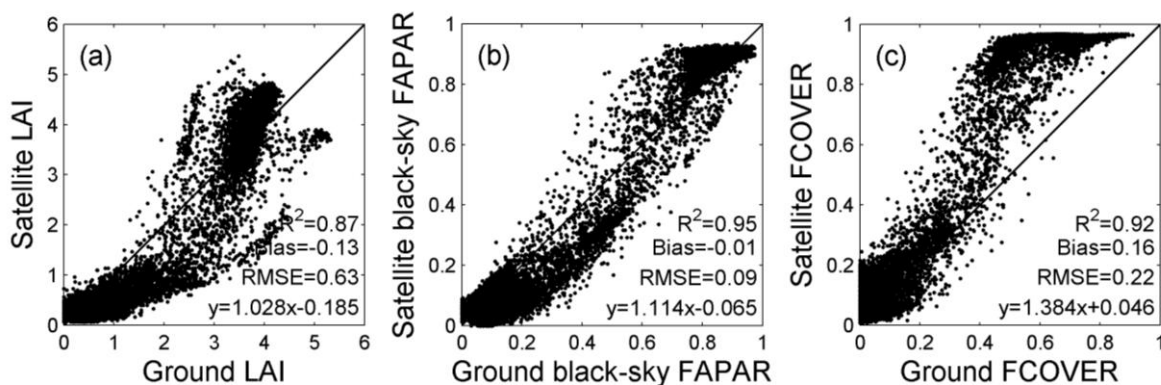

Figure 18. Direct validation of (a) LAI, (b) black-sky FAPAR, and (c) FCover Landsat-8 products (26/05/2014) with high spatial resolution ground measurements map (29/05/2014) on BARRAX site.

Comparing with the ground-based maps, Landsat-8 products show a quite good correspondence (Figure 18, R^2>0.85) for all products, but obvious bias for FCover at higher values as observed in Rosasco. Conversely to Landsat-8 products that provide LAI values up to 5, which seems quite reasonable when observing crops at decametric resolution, the ground LAI seems to saturate for LAI values higher than 3.5.

4.8. CONCLUSION

Comparison with ground measurements shows that Landsat-8 biophysical products perform good quality over most of the sites and biomes. However, the products have a bias over paddy rice fields on ROSASCO site. This will be further validated using more dates data. The influence of the background like paddy rice to the training database and inversion will be studied further.

5. ACKNOWLEDGEMENT

6. REFERENCES

Bacour, C., Jacquemoud, S., Tourbier, Y., Dechambre, M., & Frangi, J.-P. (2002). Design and analysis of numerical experiments to compare four canopy reflectance models. *Remote Sensing of Environment, 79*, 72-83

Baret, F., Bacour, C., Weiss, M., Pavageau, K., Béal, D., Bruniquel, V., Regner, P., Moreno, J., Gonzalez, C., & Chen, J. (2004). Canopy biophysical variables estimation from MERIS observations based on neural networks and radiative transfer modelling: principles and validation. In, *ENVISAT workshop*. Salzburg (Austria)

Baret, F., Hagolle, O., Geiger, B., Bicheron, P., Miras, B., Huc, M., Berthelot, B., Niño, F., Weiss, M., Samain, O., Roujean, J.L., & Leroy, M. (2007). LAI, fAPAR and fCover CYCLOPES global products derived from VEGETATION Part 1: Principles of the algorithm. *Remote Sensing of Environment, 110*, 275-286

Baret , F., Hagolle, O., Geiger, B., Bicheron, P., Miras, B., Huc, M., Berthelot, B., Weiss, M., Samain, O., Roujean, J.L., & Leroy, M. (2007). LAI, fAPAR and fCover CYCLOPES global products derived from VEGETATION. Part 1: Principles of the algorithm. *Remote Sensing of Enviroment, 110*, 275-286

Baret, F., Weiss, M., Bicheron, P., & Bethelot, B. (2009). S2PAD - Sentinel-2 MSI - Level 2B Products Algorithm Theoretical Basis Document

Baret, F., Weiss, M., Lacaze, R., Camacho, F., Makhmara, H., Pacholcyzk, P., & Smets, B. (2013). GEOV1: LAI and FAPAR essential climate variables and FCOVER global time series capitalizing over existing products. Part1: Principles of development and production. *Remote Sensing of Environment, 137*, 299-309

Camacho, F., Cernicharo, J., Lacaze, R., Baret, F., & Weiss, M. (2013). GEOV1: LAI, FAPAR essential climate variables and FCOVER global time series capitalizing over existing products. Part 2: Validation and intercomparison with reference products. *Remote Sensing of Environment, 137*, 310-329

Campbell, G.S. (1986). Extinction coefficients for radiation in plant canopies calculated using an ellipsoidal inclination angle distribution. *Agricultural and forest meteorology, 36*, 317-321

Chen, J.M., Menges, C.H., & Leblanc, S.G. (2005). Global mapping of foliage clumping index using multi-angular satellite data. *Remote Sensing of Environment, 97*, 447-457

Fourty, T., & Baret, F. (1997). Amelioration de la precision des coefficients d'absorption specifique de la matiere seche et des pigments photosynthetiques. In, *Bioclimatologie*. Avignon: INRA

Garrigues, S., Allard, D., Baret, F., & Weiss, M. (2006). Influence of landscape spatial heterogeneity on the non-linear estimation of leaf area index from moderate spatial resolution remote sensing data. *Remote Sensing of Environment, 105*, 286-298

Garrigues, S., Lacaze, R., Baret, F., Morisette, J., Weiss, M., Nickeson, J., Fernandes, R., Plummer, S., Shabanov, N.V., Myneni, R., & Yang, W. (2008). Validation and

Intercomparison of Global Leaf Area Index Products Derived From Remote Sensing Data. *Journal of Geophysical Research, 113*

GCOS (2011). Systematic Observation Requirements for Satellite-based Data Products for Climate

Hagolle, O., Dedieu, G., Mougenot, B., Debaecker, V., Duchemin, B., & Meygret, A. (2008). Correction of aerosol effects on multi-temporal images acquired with constant viewing angles: Application to Formosat-2 images. *Remote Sensing of Environment, 112*, 1689-1701

Hagolle, O., Huc, M., Pascual, D.V., & Dedieu, G. (2010). A multi-temporal method for cloud detection, applied to FORMOSAT-2, VENµS, LANDSAT and SENTINEL-2 images. *Remote Sensing of Environment, 114*, 1747-1755

Jacquemoud, S., & Baret, F. (1990). PROSPECT: A Model of Leaf Optical Properties Spectra. *Remote Sensing of Environment, 34*, 75-91

Jacquemoud, S., Verhoef, W., Baret, F., Bacour, C., Zarco-Tejada, P.J., Asner, G.P., François, C., & Ustin, S.L. (2009). PROSPECT+SAIL models: A review of use for vegetation characterization. *Remote Sensing of Environment, 113*, 56-66

Kuusk, A. (1991). Determination of Vegetation Canopy Parameters from Optical Measurements. *Remote Sensing of Environment, 37*, 207-218

Latorre, C., Camacho, F., Boschetti, M., Busetto, L., Nutini, F., Fontanelli, G., & Ranghetti, L. (2014a). Vegetation field data and production of ground-based maps: "ROSASCO site, PAVIA, ITALY" 3rd July 2014

Latorre, C., Camacho, F., Cruz, F.d.l., & Atienzar, F. (2014b). Vegetation field data and production of ground-based maps: "LAS TIESAS - BARRAX site, ALBACETE, SPAIN" 29th-30th MAY 2014

Latorre, C., Camacho, F., Pérez, M., Beget, M.E., & Bella, C.D. (2014c). Vegeration field data and production of ground-based maps: " 25 DE MAYO site, LA PAMPA, ARGENTINA" 7th- 9th February 2014

Latorre, C., Piñó, M.d.C., Camacho, F., Kussul, N., Skakun, S., Kolotii, A., & Shelestov, A. (2014d). Vegetation field data and production of ground-based maps: "PSHENICHNE site, UKRAINE", 12th June, 31st July 2014

Li, W., Weiss, M., Waldner, F., Defourny, P., Demarez, V., Morin, D., Hagolle, O., & Baret, F. (2015). Deriving LAI, FAPAR essential climate variables and FCOVER from SPOT and LANDSAT sensors: evaluation of the consistency and comparison with ground measurements. *Remote Sensing, under review*

Liu, W., Baret, F., Gu, X., Zhang, B., Tong, Q., & Zheng, L. (2003). Evaluation of methods for soil surface moisture estimation from reflectance data. *International Journal of Remote Sensing, 24*, 2069-2083

McCallum, I., Wagner, W., Schmullius, C., Shvidenko, A., Obersteiner, M., Fritz, S., & Nilsson, S. (2009). Satellite-based terrestrial production efficiency modeling. *Carbon Balance and Management, 4*

Morisette, J.T., Baret, F., Privette, J.L., & Myneni, R.B. (2006). Validation ·of Global Moderate-Resolution LAI Products: A Framework Proposed Within the CEOS Land Product Validation Subgroup. *IEEE Transactions on Geoscience and Remote Sensing, 44*, 1804-1817

Ngia, L.S.H., & Sjoberg, J. (2000). Efficient training of neural nets for nonlinear adaptive filtering using a recursive Levenberg–Marquardt algorithm. *IEEE Transactions on Signal Processing, 48*, 1915-1927

Prince, S.D. (1991). Amodel of regional primary production for use with course resolution satellite data. *International Journal of Remote Sensing, 12*, 1313-1330

Rummelhart, D.E., Hinton, G.E., & Williams, R.J. (1986). Learning internal representations by error propagation. *Parallel data processing* (pp. 318-362). MA, USA M.I.T.: Cambridge

Sánchez, J., Sendra, V., Camacho, F., Demarez, V., & Morin, D. (2014). Vegetation field data and production of ground-based maps: SOUTHTH WEST site, France June-September, 2013

Sendra, V., Latorre, C., Camacho, F., Sánchez, J., Haro, J.G., Campos-Taberner, M., & Martínez, B. (2014). Vegetation field data and production of ground-based maps:"ALBUFERA site, VALENCIA, SPAIN" June - August 2014

Verger, A., Baret , F., & Camacho de Coca, F. (2011a). Optimal modalities for radiative transfer-neural network estimation of canopy biophysical characteristics: evaluation over an agricultural area with CHRIS/PROBA observations. *Remote Sensing of Environment, 115*, 415-426

Verger, A., Baret, F., & Camacho, F. (2011b). Optimal modalities for radiative transfer-neural network estimation of canopy biophysical characteristics: Evaluation over an agricultural area with CHRIS/PROBA observations. *Remote Sensing of Environment, 115*, 415-426

Verger, A., Baret, F., & Weiss, M. (2014). Near Real-Time Vegetation Monitoring at Global Scale. *JSTARS , IEEE Journal of Selected Topics in Applied Earth Observations and Remote Sensing, 7*, 3473-3481

Verhoef, W. (1984). Light Scattering by Leaf Layers with Application to Canopy Reflectance Modeling: The SAIL Model. *Remote Sensing of Environment, 16*, 125-141

Weiss, M., & Baret, F. (2010). CAN-EYE V6.1 User Manual

Weiss, M., Baret , F., Garrigues, S., Lacaze, R., & Bicheron, P. (2007). LAI, fAPAR and fCover CYCLOPES global products derived from VEGETATION. part 2: Validation and comparison with MODIS Collection 4 products. *Remote Sensing of Environment, 110*, 317-331

Weiss, M., Baret, F., Myneni, R.B., Pragnère, A., & Knyazikhin, Y. (2000). Investigation of a model inversion technique to estimate canopy biophysical variables from spectral and directional reflectance data. *Agronomie, 20*, 3-22